

Statistical Downscaling of Coastal Directional Wave Spectra Using Deep Learning

Tianxiang Gao¹, Haoyu Jiang^{*1, 2, 3}

¹ Hubei Key Laboratory of Marine Geological Resources, China University of Geosciences, Wuhan, China

² Laboratory for Regional Oceanography and Numerical Modeling, Qingdao National Laboratory for Marine Science and Technology, Qingdao, China

³ Shenzhen Research Institute, China University of Geosciences, Shenzhen, China

Corresponding author: Haoyu Jiang (Haoyujiang@cug.edu.cn)

Key Points:

- A deep learning-based method to downscale open ocean directional wave spectra to coastal regions
- The method gives reliable coastal directional wave spectra with low computational costs and is useful for wave climate studies

Abstract

The modelling of coastal Directional Wave Spectra (DWSs) often requires downscaling techniques integrating DWSs from open ocean boundaries. Dynamic downscaling methods reliant on numerical wave models are often computationally expensive. In coastal areas, wave dynamics are strongly influenced by the topography, implying that once the DWSs at the open ocean boundary are known, the DWSs at various locations along the coast are almost determined. This property can be utilized for statistical downscaling of coastal DWSs. This study presents a deep learning approach that can compute coastal DWSs from open ocean DWSs. The performance of the proposed downscaling model was evaluated using both numerical wave model data and buoy data in the Southern California Bight. The results show that the deep learning approach can effectively and efficiently downscale coastal DWSs without relying on any predefined spectral shapes, thereby holding promise for coastal wave climate studies.

Plain Language Summary

The directional Wave Spectrum (DWS) describes the distribution of wave energy among different frequencies and directions. It is important for many practical applications such as the design of coastal structures and hazard assessment. Modelling of coastal DWSs often involves running a regional numerical wave model, which is very computationally intensive. This study introduces a deep learning method to accurately predict coastal DWSs using open ocean wave data, reducing computational costs. By leveraging the influence of topography on wave dynamics, the model downscales DWSs along the coast. Tested by a case study in the Southern California Bight, the approach proves effective. This advancement offers a promising tool for studying coastal wave climates in future climate scenarios.

1 Introduction

Wind-generated surface gravity waves (hereafter, waves) are the most ubiquitous phenomenon observable on the sea surface. Directional Wave Spectra (DWSs), as a fundamental tool for studying and describing waves, have been widely used in studies of waves and related ocean/coast engineering. In contrast to the conventional usage of Integral Wave Parameters (IWPs) such as Significant Wave Height (SWH), Mean Wave Direction (MWD), and Mean Wave Period (MWP), which provide only a limited description of the wave field and can be misleading in sea states with multiple wave components, DWSs can depict the distribution of wave energy across different frequencies and directions. They have the capability to differentiate waves from different origins, making them a detailed and comprehensive tool for describing waves (e.g., Holthuijsen 2007). Therefore, the effective acquisition of wave spectra is of significant importance for both scientific research and human activity.

DWSs in coastal areas can provide vital information for the protection of coastal infrastructure, the study of beach morphology evolution, and wave climate research. Hence, employing downscaling methods to obtain local DWSs using data from offshore waves holds paramount importance for both coastal engineering and wave climate studies. Compared to the DWS in coastal regions, the DWS in the open ocean is relatively easy to obtain through numerical modelling (e.g., Alday et al. 2021), statistical modelling (e.g., Song and Jiang 2023), or remote sensing (e.g., Jiang et al. 2022). Once DWSs in the open ocean boundary are obtained,

coastal DWSs can then be modelled using a higher-resolution numerical wave model (NWM), which is often termed dynamic downscaling. However, the dynamic downscaling approach is subject to computational resource constraints, limiting its scope of application and efficiency. Therefore, several statistical downscaling methods with low computational costs were presented as a more efficient and economical alternative (e.g., Hegermiller 2017a, James et al. 2018, Ricondo et al. 2023).

Topographic modulation, including land shadowing, shoaling, refraction, bottom friction, depth-induced breaking, plays the most important role in the evolution and variability of nearshore DWSs. Given that topography is a relatively stable factor, a strong correspondence can be established between the nearshore DWSs and the open ocean DWSs once the topography is determined. When the DWS at the ocean boundary is ascertained, the corresponding nearshore DWS can also be essentially determined. This can be regarded as the theoretical basis for statistical downscaling. However, such an implicit mapping relationship from the open ocean boundary to the nearshore DWSs might entail a certain level of nonlinearity and complexity.

In recent years, machine learning technologies, especially the fast-developing deep learning (DL), have opened new avenues for such problems. The DL methods can “learn” the features and correlations between inputs and outputs from a large amount of data by supervised training. They are well suited for the problem that there are quantitative relationship inputs and outputs but the relationship is complex in its explicit form. Due to its powerful ability in nonlinear regression, DL has been widely used in many aspects of oceanography (e.g., Ham et al. 2019, Jiang 2022), including modelling ocean waves (e.g., James et al. 2018, Song and Jiang 2023). Regarding DL-based downscaling, James et al. (2018) showed that DL is able to statistically downscale the bulk wave parameters very efficiently in a semi-closed basin, which can serve as a surrogate to NWMs. Song and Jiang (2023) show that DL has the capability to predict single-point DWSs in open oceans with (both local current and remote historical) wind forcing with low computational costs. When abstracting the problem of statistical downscaling of DWSs at a given point, we find that deep learning seems to be a good tool for digging such complex quantitative relationships between input (DWSs in the open ocean boundary) and output (DWSs at a given coastal location).

In this paper, we establish a statistical model to downscale DWSs from the open ocean boundary to a coastal location based on a UNet architecture. The model can capture the topographic modulations on DWSs all at once from the data, resulting in accurate results while significantly reducing computational costs compared to traditional dynamic downscaling methods. It is noted that the aim of all such statistical models is not to replace physics-based NWMs, but rather to serve as a faster data-driven surrogate that is applicable for time-sensitive applications and computational resource-limited applications. Through this study, we aim to showcase the potential of DL in the application of DWS downscaling, providing insightful perspectives and inspiration for future research. The structure of this paper is as follows: Section 2 introduces the study area, the dataset employed, and the UNet model architecture. Section 3 presents and analyzes the experimental results. Section 4 discusses and summarizes the findings.

2 Study Area, Data, and Methods

2.1 Study Area

The study area selected for this study is the Southern California Bight (SCB, Figure 1a), located along the western coast of the United States, spanning from Point Conception to the Mexican border. The SCB is characterized by complex and dynamic wave conditions, making it a focal area for wave research. The wave climate in this region is predominantly influenced by swells originating from Westerlies of both North and South Pacific, as well as local wind seas (Jiang 2020). These wave systems all exhibit temporal variability across various scales, including seasonal, inter-annual, and long-term trends (Jiang and Mu 2019). Moreover, the wave conditions here are significantly modulated (including wave refraction, diffraction, and sheltering) by the highly irregular shelf topography and many geographical features such as Santa Rosa Island (SRI), Santa Cruz Island (SCI), and Santa Catalina Island (CI), leading to substantial small-scale coastal variations in nearshore wave energy (e.g., Hegermiller et al. 2017b). This area can be regarded as an ideal location for the study of DWS downscaling techniques, given the extensive transformation of the coastal DWSs. By statistically downscaling DWSs in the SCB, we aim to enhance our ability to predict nearshore wave conditions and to provide robust tools for DWS downscaling in similar complex coastal environments worldwide.

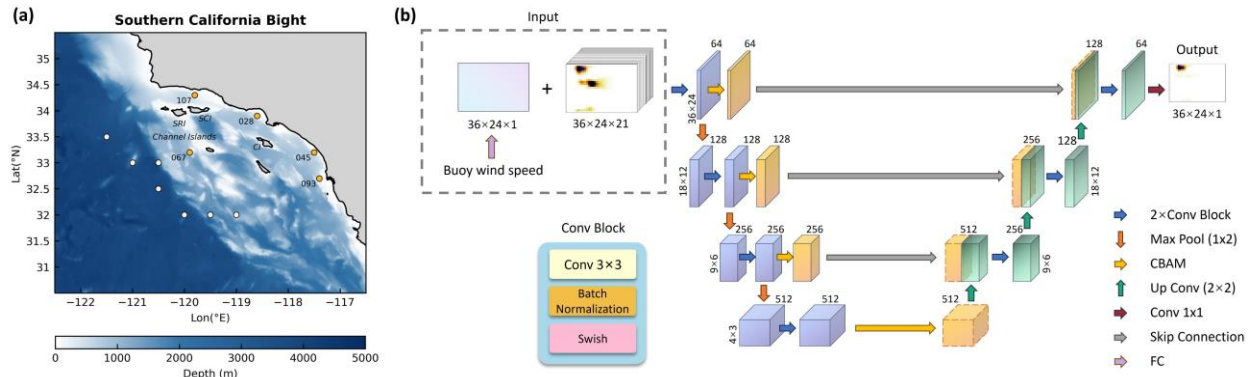


Figure 1. The study area and the architecture of the UNet model used in this study. (a) The bathymetry of the Southern California Bight (Bathymetric data are from ETOPO 2022, NOAA NCEI 2022, which is available at: <https://www.ncei.noaa.gov/products/etopo-global-relief-model>). The five orange circles represent the locations of five CDIP buoys where directional wave spectra are available from both the IOWAGA dataset and CDIP dataset (see Section 2.2). The seven white points denotes the locations of open ocean directional wave spectra that are used as model input in this study. (b) An illustration of the UNet architecture used in this study. The input data comprise 21 directional wave spectra from 7 different boundary locations and three time points (zero, three, and six hours before the current time), plus the wind vector from buoy points. Each directional wave spectrum is represented in a format with a width of 24 (directions) and a height of 36 (frequencies), corresponding to outputs for the IOWAGA dataset. The dimensional attributes of the wind data obtained from buoy points are transformed through a fully connected neural network layer to ensure alignment with the dimensional structure of the wave spectrum. Each colored cube symbolizes a feature map, with the numbers on the left and right sides indicating the width \times height dimensions, and the numbers at the top representing the number of channels. The blue arrows denote two Conv-Blocks, with each Conv-Block comprising a 3×3 convolution, batch normalization, and Swish activation function, as depicted in

the lower left module. The orange arrows represent a 2×2 max pooling operation, while the green arrows indicate an up-convolution operation. The red arrows signify a 1×1 convolution, and the gray arrows represent skip connections, which entail the concatenation of features. The final output of the model is the predicted DWS with also 24 directions and 36 frequencies.

2.2 Data

Nowadays, there are several global datasets of DWS with coarse resolution, such as ERA5 wave (Hersbach et al. 2020), CAWCR (Centre for Australian Weather and Climate Research) wave hindcast (Smith et al. 2020), and IOWAGA (Integrated Ocean Waves for Geophysical and other Applications) hindcast (Alday et al. 2021). IOWAGA is a global hindcast wave field dataset generated using the WAVEWATCH III® model (WW3DG 2019). This hindcast is run with the physical parameterization of Ardhuin et al. (2010) forced by the global 10-m-wind data from the ERA5 dataset, surface current fields from the CMEMS-Globcurrent, and ice concentration from the IFREMER SSMI-derived daily product. Without assimilating wave observations, the data showed good agreement with both buoy and altimeter measurements. The DWS in this wave model are discretized in 24 directions (15° directional resolution) and 36 frequencies exponentially spaced from 0.034 to 0.95 Hz with a 1.1 increment factor from one frequency to the next. The global model was with a resolution of $0.5^\circ \times 3h$. This dataset contains not only the integrated (and partitioned) wave parameters, but also DWSs at more than 10,000 points all along the world coastline plus the locations of moored buoys (including those in Figure 1) and some additional offshore points. In the study area, a two-way nested grid with a higher resolution of $1/6^\circ$ was used and the wave data were dynamically downscaled. The dataset is available from the website of Laboratoire d'Océanographie Physique et Spatiale (LOPS), IFREMER (<https://www.umar-lops.fr/Donnees/Vagues>) and more details can be found in Alday et al. (2021).

The Coastal Data Information Program (CDIP) constitutes an extensive network designed for monitoring wave and beach conditions along the United States coastline. The program has strategically positioned and maintained wave buoys at different locations. These directional wave buoys are capable of measuring waves with periods ranging from 1.6 to 30 seconds. The wave spectrum data of these buoys encompasses 64 frequencies, ranging from 0.025Hz to 0.58Hz. For each of these frequencies, the CDIP provides the first five Fourier coefficients of waves (“First-5”) which are the minimum requirement for reconstructing directional wave spectra. In this study, buoy DWSs were reconstructed using the Maximum Entropy Method from the aforementioned “First-5” (Earle et al., 1999). It is noted that different reconstruction method can result in different DWSs, and these methods have problems such as reducing the directional spread and generating spurious peaks. Also, the buoy-reconstructed DWSs are often noisy with respect to spectral densities at different frequency-direction bins (e.g., Jiang et al., 2022), but they can give a good reference for the spectral shape and the IWPs from buoys, especially SWHs, are reliable. All data and products associated with the CDIP are accessible via the CDIP THREDDS server (<http://thredds.cdip.ucsd.edu/>). More details of this dataset are available in Behrens et al. (2024).

We select the data of IOWAGA DWSs at seven open ocean points ($121.5^\circ W$, $33.5^\circ N$; $121.0^\circ W$, $33.0^\circ N$; $120.5^\circ W$, $33.0^\circ N$; $120.5^\circ W$, $32.5^\circ N$; $120.0^\circ W$, $32.0^\circ N$; $119.5^\circ W$, $32.0^\circ N$; and $119.0^\circ W$, $32.0^\circ N$) as the input for the DL model. The DWSs at five buoy locations, namely

CDIP067, CDIP028, CDIP045, CDIP093, and CDIP107, are used for training and evaluating the DL downscaling model. The locations of these input and output points are shown in Figure 1a.

Downscaling process itself is often regarded as a model-to-model (a coarse-resolution one to a fine-resolution one) problem. Therefore, the IOWAGA DWSs at these buoy locations are used as the target output to train and evaluate the DL downscaling model. Meanwhile, we also used the CDIP buoy-reconstructed DWSs directly as the output to show that this DL model can also directly downscale the coarse-resolution modelled DWSs using in-situ observations.

2.3 Methods

The UNet architecture has emerged as a significant advancement in in medical image segmentation (Ronneberger et al. 2015). In this study, we employ the UNet architecture with modifications aimed at enhancing its performance. Firstly, we incorporate the CBAM (Convolutional Block Attention Module) attention mechanism (Woo et al. 2018) into the encoder section, enabling the network to focus more intently on the important features within the DWSs. Secondly, we substitute the ReLU activation function in each convolutional block with the Swish activation function (Ramachandran et al. 2017) and adopted the Lion optimizer (Chen et al. 2023). These enhancements are intended to improve the model's generalization capabilities, enhance prediction accuracy, and expedite the training process.

As illustrated in Figure 1b, the UNet architecture in this study comprises a U-shaped encoder-decoder structure. Given the dimensions of the input data, we have employed three encoder-decoder modules in this instance. The input data is of the size $[24, 36, 7 \times 3 + 1]$ denoting 24 directions, 36 frequencies, 7 open ocean locations, 3 time points (zero, three, and six hours before the current time, to take the wave propagation time into consideration), plus 1 wind vector record at the target location that is then transformed into a 24×36 matrix through a fully connected neural network. This wind vector is to capture the high-frequency tails that are primarily impacted by local wind at the target location rather than boundary conditions.

The foundational module of the UNet network comprises two Conv-Blocks, each comprising a 3×3 two-dimensional convolutional layer, followed by a BatchNorm2d layer and a Swish activation function. The encoder section (left half of Figure 1b) is composed of double convolutional blocks, a CBAM, and max pooling. This arrangement progressively compresses the dimensions of the feature map in terms of both length and width, thereby enhancing higher-order features. The CBAM serves to amplify crucial features while simultaneously suppressing less important features at the respective scale of the image. These features are then fed back to the corresponding up-sampling portion of the network through skip connections, enabling the model to generate output utilizing multiple input scales. Following the encoder, an equivalent number of decoders (right half of Figure 1b) decode the features, including up-sampling to double the size of the feature map and skip connections. This process yields a feature map of the size $[24, 36, 64]$. The final layer of the model consists of a 1×1 convolutional layer which reduces the number of channels to 1, producing the final 24×36 DWS output of the model.

For each buoy location, we utilize data spanning 29 years from 1993 to 2021, dividing it into training (1993-2015) and testing (2016-2021) sets. Prior to inputting the DWS data into the network, we randomly shuffle samples within the training set. The value ranges of spectral densities vary significantly for different frequencies and directions bins. Therefore, we apply the Min-Max scaling normalization (normalizing the data in every spectral bin into the range $[0, 1]$)

to each spectral bin to mitigate the scale sensitivity and accelerate the convergence of model training.

The loss function is the Mean Squared Error (MSE) between the predicted and actual values of the normalized wave spectral densities. The MSE is computed as follows:

$$MSE = \frac{1}{m} \sum_{i=1}^m (y_{pre}^i - y_{true}^i)^2 \quad (1)$$

where m represents the number of samples, y_{pre}^i denotes the predicted value from the model output for the i -th spectral bin, and y_{true}^i is the reference value of the wave spectrum (IOWAGA-downscaled or buoy-measured) for the i -th spectral bin.

The model training process is configured to run a maximum of 100 epochs. To enhance training efficiency and mitigate overfitting, we employ an early stopping strategy, i.e., if no reduction in the loss on the validation set is observed for 10 consecutive epochs, the training is halted. Moreover, to further optimize the performance of the model, we employ a dynamic learning rate adjustment strategy. The initial learning rate is set to 10^{-4} , and if the loss on the training set does not decrease for 4 epochs, we reduce the learning rate to one-tenth of its previous value. To prevent the learning rate from becoming excessively small, potentially halt training, we set a lower limit for the learning rate at 10^{-7} . All training experiments converged before reaching the preset maximum of 100 epochs, meeting the early stopping criteria.

The training was conducted separately on five buoy points within the IOWAGA and CDIP datasets, resulting in a total of ten models. All models were trained from scratch, and the model training was conducted on a single NVIDIA 3080Ti graphics card, with Ubuntu 22.04 LTS serving as the operating system. The code of UNet is implemented using Python 3.10. The training duration for each buoy point model is within one hour, and it takes only several seconds to downscale 6-year data at each location using the trained model.

3 Results

First, we use the IOWAGA DWSs at the buoy locations to assess whether the DL downscaling model can reproduce the dynamic downscaling in the NWM within acceptable error margins. Taking the CDIP028 buoy location as an example, the five rows in Figure 2 are: the DWSs from its nearest open boundary point (120.5°W, 33.0°N) before downscaling, dynamically downscaled IOWAGA DWSs, DL-downscaled DWSs using IOWAGA DWSs as training targets, buoy-reconstructed DWSs, and DL-downscaled DWSs using buoy DWSs as training targets, respectively. For each row, the four columns to the left of the dashed line are the corresponding DWSs at four arbitrarily selected time points (12:00:00T on the 1st of Jan, April, July, and October, 2020), followed by the corresponding Annual Mean DWS (AMDWS) in 2020 to the right of the dashed line.

The comparison between the 1st and 2nd rows shows that the shapes of the DWSs in the coastal region can be largely different from the DWSs in the open ocean due to the coastal processes, even if the two locations are not far away (~250 km) from each other. For the DWSs at the open ocean point, they often contain narrow peaks at $-20^\circ \sim 20^\circ$ corresponding to the swells coming from the westerlies of the South Pacific, which appears as only one peak in the AMDWS. Another more prominent feature in DWSs in the open ocean location is the southeastward peaks, which partly correspond to swells coming from the North Pacific

westerlies and partly correspond to wind-seas generated locally by California low-level coastal jets. These two systems also appear as only one peak in the AMDWS. Besides, low-energy southward low-frequency partitions can also be observed in some cases but not in the AMDWS because their energy is smoothed and overwhelmed by wave systems with larger spectral densities.

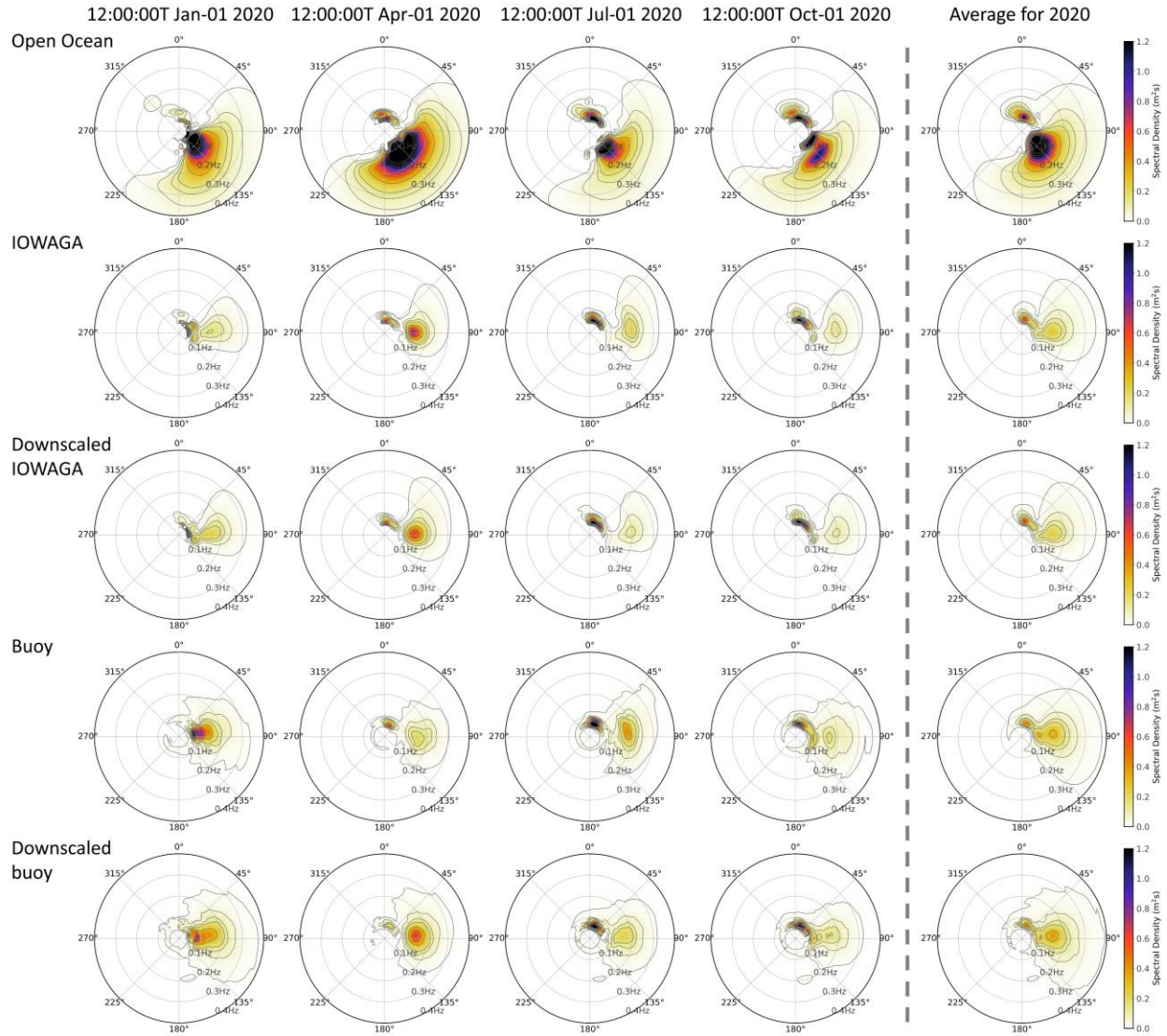


Figure 2. The comparison of directional wave spectra (DWSs) from different data sources at the location of buoy CDIP028. The 1st row is the DWSs at the open boundary point (120.5°W, 33.0°N) before downscaling. The 2nd row shows the corresponding DWSs from IOWAGA at the buoy location, and the 3rd row shows the results from the DL downscaling model using IOWAGA DWSs as the training target. The 4th row is the corresponding buoy reconstructed DWSs, and the 5th row is the results from the DL downscaling model using buoy DWSs as the training target. The four columns to the left of the dashed line in each row are the corresponding DWSs at four arbitrarily selected time points. The five DWSs to the right of the dashed line in each row are the corresponding annual mean DWSs in 2020.

As waves in the open ocean propagate to the coastal regions (2nd row), energy attenuation and refraction occur. At the CDIP028 location, positions of peaks corresponding to northward swells experience only small changes, and their corresponding peak in the AMDWS remain largely unchanged, albeit with substantially reduced spectral densities. Meanwhile, the southeastward waves, both wind-seas and swells, are refracted significantly to eastward ones, accompanied by considerable energy reduction. Moreover, low-energy southward partitions in the open ocean point disappear in the coastal location due to the impact of local topography.

Comparing the 2nd and the 3rd rows in Figure 2, it can be seen that the DL downscaling model can well capture the features of spectral evolution. For both individual instantaneous DWSs and AMDWS, the DL-downscaled DWSs have a good visual agreement with those derived from dynamic downscaling with respect to both spectral shape and energy level. Particularly, spectral bins with relatively high energy densities are accurately modeled, with well-captured spectral peaks. To save space, the results at the rest four locations are only shown in Figures S1-S5 in the Supporting Information (SI). These figures also show that the coastal DWSs obtained by the DL model have a good agreement with those from dynamic downscaling.

To further evaluate the performance of the DL downscaling model from a statistical point of view, three IWPs, including the SWH, MWP, and MWD, are computed from the dynamic downscaling method and the DL downscaling model, and are then compared. As mentioned in Section 1, these IWPs provide only a limited description of the wave and can be sometimes misleading in sea states with multiple wave components. Also, two spectra with different shapes can sometimes have the same IWP. However, Figure 2 and Figures S1-S5 have shown that the spectral shapes derived from the two methods have a good agreement in general. This consistency in spectral shape guarantees the comparison of IWPs to be a reasonable way to evaluate the performance of the DL downscaling model. These IWPs, especially SWH, are also widely used in the verification of NWMs because high-quality SWH measurements are available from space-borne altimeters (e.g., Alday et al. 2021; Liu et al. 2021). For a more detailed quantitative assessment, the bias, Root-Mean-Square Error (RMSE), and Correlation Coefficient (CC) are used as the error metrics to evaluate the performance of the DL downscaling model:

$$Bias = \frac{1}{n} \sum_{i=1}^n (y_i - x_i) \quad (2)$$

$$RMSE = \sqrt{\frac{1}{n} \sum_{i=1}^n (y_i - x_i)^2} \quad (3)$$

$$CC = \frac{\sum_{i=1}^n (y_i - \bar{y})(x_i - \bar{x})}{\sqrt{\sum_{i=1}^n (y_i - \bar{y})^2} \sqrt{\sum_{i=1}^n (x_i - \bar{x})^2}} \quad (4)$$

where x and y denote the IWPs or spectral density from the reference data and the DL models, respectively, and the bars over them denote their mean values.

Figure 3a shows the scatter plot between DL-downscaled and dynamically downscaled spectral densities at all spectral bins at the location of buoy CDIP028 (all data are from the test set). Although such a direct comparison between spectral densities is not typically recommended for evaluating the agreement between two DWSs due to the so-called “double penalty effect” (a small difference in the location of narrow swell spectral peaks can lead to a large difference in spectral density), it still provides a quantitative reference on the performance of the DL downscaling model. The CC between the spectral densities from dynamic downscaling and DL downscaling is ~ 0.98 , which seems to be a good agreement compared to the CC of spectral

densities between two smoothed buoy-reconstructed DWSs (Jiang et al. 2022) and the CC of spectral densities in Song and Jiang (2023).

Figures 3b-3d show the corresponding scatter plots for SWH, MWD, and MWP, respectively, between the two downscaling methods. Again, the overall results of the three IWP all exhibit high overall accuracy: The CCs for SWH, MWD, and MWP all reached 0.98; the biases for SWH, MWD, and MWP are ~ 0.01 m, $\sim 0.4^\circ$, and ~ 0.04 s, respectively; and the corresponding RMSEs are ~ 0.06 m, $\sim 3.3^\circ$, and ~ 0.44 s, respectively. Nearly all data points lie perfectly along the $y = x$ line except for several outliers in the MWD scatter plot. These outliers correspond to the condition that the overall wave energy is low, in which a small energy error from the model can have a large impact on the estimation of MWD. The results at the rest four locations are shown in Figures S6-S10 in the SI where the error metrics of the results from the DL models are similar to those in Figures 3a-3d. The CCs of the three IWPs in the four points vary from 0.97 to 1.00, again affirming the consistency of results between the DL downscaling method and dynamic downscaling.

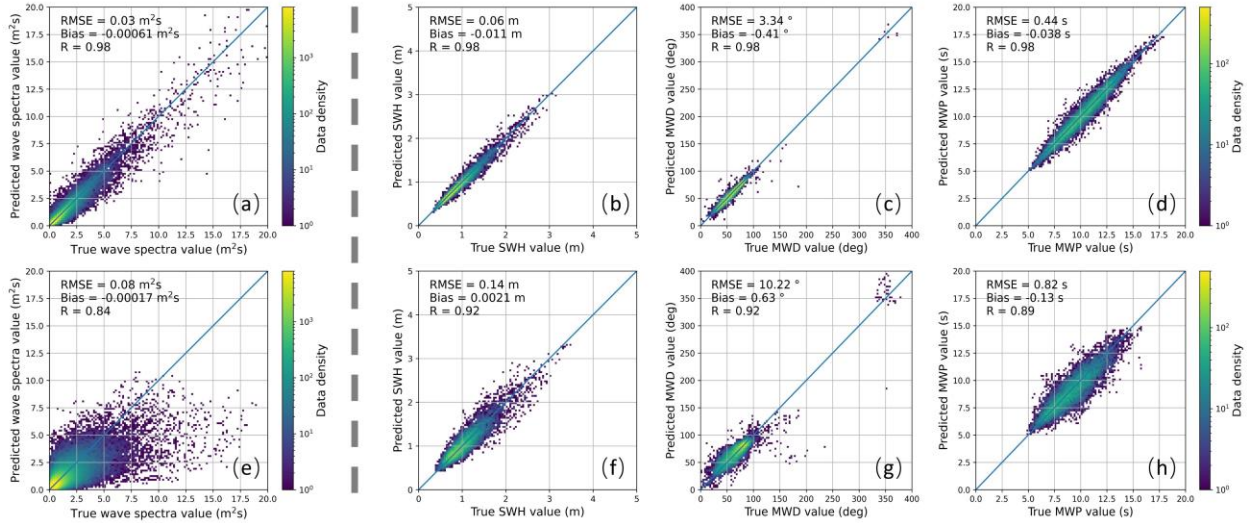


Figure 3. Scatter plots between DL downscaling results and their corresponding reference data at the location of buoy CDIP028. The 1st row is the comparison between DL-downscaled results (using IOWAGA DWS as training targets) and dynamic-downscaled results, and the 2nd row is the comparison between DL-downscaled results (using buoy DWS as training targets) and buoy data. The four columns are the comparison for (a & e) spectral densities, (b & f) SWH, (c & g) MWD, and (d & h) MWP, respectively.

According to the rationale of the DL downscaling method, the downscaling model can also be trained directly using in-situ observations as targets. Some cases of buoy-reconstructed and corresponding DL-downscaled DWSs (using buoy DWSs as training targets) for buoy CDIP028 are shown in the 4th and 5th rows of Figure 2, respectively. The results for the other buoys are shown in Figures S11-S14. Compared to the DWSs from IOWAGA, the energy ratio of the wind wave system is slightly higher in the downscaling results of the model, and the swell is wider due to scattering effects (Jiang et al. 2016, Smit et al. 2018). Besides, the buoy-reconstructed DWSs themselves are much noisier than modelled DWSs. The noises in DWSs lead to a strong “double penalty effect” which then results in a CC of only 0.84 between DL-downscaled and buoy-reconstructed spectral densities (Figure 3e), which is much lower than the value of 0.98 derived from the “model-to-model” downscaling in Figure 3a. However, the DL

downscaling method can still well capture the main shapes and the energy levels of the buoy-reconstructed DWSs for both wind-sea and swell systems. Also, the SWH, MWD, and MWP are in good agreement with the buoy-measured ones: The CCs/RMSEs for SWH, MWD, and MWP are $\sim 0.92/0.14$ m, $0.92/10.22^\circ$, and $0.89/0.82$ s, respectively. Although the agreement is not as good as the comparison between DL and dynamic downscaling, this accuracy is not bad for a model-against-observation comparison. Similar accuracy is observed in the comparisons of IWPs for other buoys, as depicted in Figures S7-S10 in the SI.

4 Discussions

As mentioned in Section 1, the rationale of the DL downscaling method presented in this study is clear: There is an implicit and complex but nearly fixed mapping relationship between the DWSs along open ocean boundaries and the DWS at a coastal location, given the topography is unchanged. This relationship can be fitted by the strong power of deep learning. This is why the DL downscaling can effectively and efficiently downscale open ocean DWSs into nearshore ones without relying on any predefined spectral shapes. However, it is also found that the agreement is better between the DL-downscaled and dynamic-downscaled results is significantly better than that between DL-downscaled and buoy-reconstructed results. This is because when the DL model is trained to downscale the IOWAGA DWSs from the open boundary to coasts, the inputs and the target outputs are more consistent. After all, they are the corresponding inputs and outputs of the NWM for downscaling. However, significant inconsistency exists between modelled open ocean DWSs and buoy DWSs. Although DL models can correct part of the inconsistency through extensive data, there remain inconsistencies that cannot be learned by DL. For instance, buoy DWSs have large random errors (Jiang et al. 2022) that can hardly be replicated by any model. In addition, except for the impact of wind and topography, the evolution of DWSs in the coastal regions is also modulated by wave-current-tide interactions. The information on currents and tides is not used as the input in our DL model (tides and tidal currents are also absent in the IOWAGA hindcast), while these impacts and modulations might be evident in buoy DWSs. It is anticipated that the accuracy of (both dynamic and DL) downscaling can be further improved if the information on currents and tides is available.

In some cases, only the information on one point or fewer points in the open ocean boundary is available, and the wind information at the target location might be unavailable. A sensitivity test is conducted to test the performance of the DL model when less input information is used. We try to reduce the number of input locations or the number of input time points to one, or eliminate the wind information as input. For each location, four sets of sensitivity tests are conducted and the corresponding results of DWSs and IWPs are shown in Figures S1-S5 and S6-S10, respectively. Although a slight decrease in model accuracy is observed with the input information reduced, the model can still have an acceptable accuracy even when only one DWS at one time point is used as input without wind information: The spectral shapes are well downscaled and the CCs/RMSEs for SWH, MWD, and MWP are $\sim 0.95/0.10$ m, $0.95/5.1^\circ$, and $0.93/0.75$ s, respectively, at the location of CDIP028 (similar performance for the rest four points).

Compared to dynamic downscaling, the DL downscaling method for DWSs presented in this study can significantly reduce computational costs while maintaining high accuracy. It can be used as a surrogate for an NWM in many time-sensitive or computational resource-limited applications. One potential application of this method is in wave climate studies. Nowadays,

more and more attentions are drawn to spectral wave climate (e.g., Espejo et al. 2014, Jiang and Mu 2019, Echevarria et al. 2019, Lobeto et al. 2022), but running ensemble high-resolution NWMs to output some coastal DWSs under many different climate scenarios for long-term projections is challenging. This DL downscaling method can rapidly process tens of thousands of sample data in seconds, allowing fast prediction of DWSs under different future scenarios. Future work can be further optimizing the DL model structure using advances in AI and including more physically related input information (such as currents and water level), which might further improve the performance of the model.

Acknowledgments

This work is jointly supported by the National Key Research and Development Program of China (2023YFC3008203), the National Natural Science Foundation of China (42376172), and the Guangdong Basic and Applied Basic Research Foundation (2022A1515240069). We would like to thank IFREMER and CDIP for sharing the data.

Availability Statement

All the data used in this study is available online: IOWAGA data is from Alday et al. (2021), and can be downloaded from the official website of LOPS, IFREMER (<https://www.umn-lops.fr/Donnees/Vagues>). CDIP data is from Behrens et al. (2024), can be download from its official website <https://cdip.ucsd.edu/>. The deep learning models are realized using PyTorch (<https://pytorch.org/>).

References

- Alday, M., Accensi, M., Ardhuin, F., Dodet, G., (2021). A global wave parameter database for geophysical applications. Part 3: improved forcing and spectral resolution. *Ocean Modelling* 166, 101848. <https://doi.org/10.1016/j.ocemod.2021.101848>
- Ardhuin, F., Rogers, E., Babanin, A.V., Filipot, J., Magne, R., Roland, A., van der Westhuysen, A., Queffelec, P., Lefevre, J., Aouf, L., Collard, F. (2010). Semiempirical Dissipation Source Functions for Ocean Waves. Part I: Definition, Calibration, and Validation. *Journal of Physical Oceanography*. 40 (9), 1917–1941. <https://doi.org/10.1175/2010JPO4324.1>
- Behrens, J., Olfe, C., Cameron, G., Bucciarelli, R., Timmerman, R., Wright, D., Lodise, J., Merrifield, S., & Terrill, E. (2024). Coastal Data Information Program: advances in measuring and modeling wave activity, climate, and extremes. *Coastal Engineering Journal*. <https://doi.org/10.1080/21664250.2024.2308021>
- Chen, X., Liang, C., Huang, D., Real, E., Wang, K., Pham, H., Dong, X., Luong, T., Hsieh, C.-J., Lu, Y., & Le, Q. V. (2024). Symbolic discovery of optimization algorithms. *Advances in Neural Information Processing Systems*, 36.
- Earle, M.D., Steele, K.E., Wang, D.W.C. (1999). Use of advanced directional wave spectra analysis methods. *Ocean Eng.* 26 (12), 1421–1434. [https://doi.org/10.1016/S0029-8018\(99\)00010-4](https://doi.org/10.1016/S0029-8018(99)00010-4)
- Echevarria, E. R., Hemer, M. A., & Holbrook, N. J. (2019). Seasonal variability of the global spectral wind wave climate. *Journal of Geophysical Research: Oceans*, 124, 2924–2939. <https://doi.org/10.1029/2018JC014620>
- Espejo, A., Camus, P., Losada, I.J., Méndez, F.J. (2014). Spectral ocean wave climate variability based on atmospheric circulation patterns. *Journal of Physical Oceanography*. 44 (8), 2139–2152. <https://doi.org/10.1175/JPO-D-13-0276.1>
- Ham, Y., Kim, J., Luo, J. (2019). Deep learning for multi-year ENSO forecasts. *Nature* 573 (7775), 568–572. <https://doi.org/10.1038/s41586-019-1559-7>
- Hegernmiller, C.A., Rueda, A., Erikson, L.H., Barnard, P.L., Antolinez, J.A.A., Mendez, F.J. (2017a). Controls of multimodal wave conditions in a complex coastal setting. *Geophysical Research Letters*, 44 (24), 312–315,

323. <https://doi.org/https://doi.org/10.1002/2017GL075272>
- Hegermiller, C.A., Antolinez, J.A.A., Rueda, A., Camus, P., Perez., J., Erikson, L.H., Barnard, P. L., Mendez, F.J. (2017b). A Multimodal Wave Spectrum–Based Approach for Statistical Downscaling of Local Wave Climate. *Journal of Physical Oceanography*, 47 (2), 375–386. <https://doi.org/10.1175/JPO-D-16-0191.1>
- Hersbach, H., Bell, B., Berrisford, P., Hirahara, S., Horányi, A., Muñoz-Sabater, J., Nicolas, J., Peubey, C., Radu, R., Schepers, D., Simmons, A., Soci, C., Abdalla, S., Abellan, X., Balsamo, G., Bechtold, P., Biavati, G., Bidlot, J., Bonavita, M., De Chiara, G., Dahlgren, P., Dee, D., Diamantakis, M., Dragani, R., Flemming, J., Forbes, R., Fuentes, M., Geer, A., Haimberger, L., Healy, S., Hogan, R.J., Hólm, E., Janisková, M., Keeley, S., Laloyaux, P., Lopez, P., Lupu, C., Radnoti, G., de Rosnay, P., Rozum, I., Vamborg, F., Villaume, S., Thépaut, J. (2020). The era5 global reanalysis. *Quarterly Journal of the Royal Meteorological Society*, 146 (730), 1999–2049. <https://doi.org/https://doi.org/10.1002/qj.3803>
- Holthuijsen, L. H. (2007). *Waves in Oceanic and Coastal Waters*. Cambridge University Press, 387pp.
- James, S.C., Zhang, Y., O'Donncha, F. (2018). A machine learning framework to forecast wave conditions. *Coastal Engineering*, 137, 1–10. <https://doi.org/https://doi.org/10.1016/j.coastaleng.2018.03.004>
- Jiang, H.Y., Mu, L. (2019). Wave climate from spectra and its connections with local and remote wind climate. *Journal of Physical Oceanography*, 49 (2), 543–559. <https://doi.org/10.1175/JPO-D-18-0149.1>
- Jiang, H., Babanin, A.V., Chen, G. (2016). Event-based validation of swell arrival time. *Journal of Physical Oceanography*, 46 (12), 3563–3569. <https://doi.org/10.1175/JPO-D-16-0208.1>
- Jiang, H., Mironov, A., Ren, L., Babanin, A.V., Wang, J., Mu, L. (2022). Validation of wave spectral partitions from swim instrument on-board cfosat against in situ data. *IEEE Trans. Geosci. Remote.*, 60, 1–13. <https://doi.org/10.1109/TGRS.2021.3110952>
- Jiang, H. (2020). Wave Climate Patterns from Spatial Tracking of Global Long-Term Ocean Wave Spectra. *Journal of Climate*, 33 (8), 3381–3393, <https://doi.org/10.1175/JCLI-D-19-0729.1>
- Jiang, H. (2022). Wind speed and direction estimation from wave spectra using deep learning. *Atmospheric Measurement Techniques*, 15, 1–9, <https://doi.org/10.5194/amt-15-1-2022>
- Liu, Q., Babanin, A.V., Rogers, W.E., Zieger, S., Young, I.R., Bidlot, J., Durrant, T., Ewans, K., Guan, C., Kirezci, C., Lemos, G., Machutchon, K., Moon, I., Rapizo, H., Ribal, A., Semedo, A., Wang, J. (2021). Global wave hindcasts using the observation-based source terms: description and validation. *Journal of Advances in Modeling Earth Systems*, 13 (8), e2021M-e2493M. <https://doi.org/10.1029/2021MS002493>
- Lobeto, H., Menendez, M., Losada, I.J., Hemer, M. (2022). The effect of climate change on wind-wave directional spectra. *Global and Planetary Change*, 213, 103820. <https://doi.org/10.1016/j.gloplacha.2022.103820>
- Ramachandran, P., Zoph, B., & Le, Q. V. (2017). Searching for activation functions. *arXiv preprint arXiv:1710.05941*.
- Ricondo, A., Cagigal, L., Rueda, A., Hoeke, R., Storlazzi, C.D., Méndez, F.J. (2023). HyWaves: Hybrid downscaling of multimodal wave spectra to nearshore areas. *Ocean Modelling*, 184, 102210. <https://doi.org/10.1016/j.ocemod.2023.102210>
- Ronneberger, O., Fischer, P., & Brox, T. (2015). U-net: Convolutional networks for biomedical image segmentation. In *Medical Image Computing and Computer-Assisted Intervention–MICCAI 2015: 18th International Conference, Munich, Germany, October 5–9, 2015, Proceedings, Part III* (pp. 234–241). Springer International Publishing. https://doi.org/10.1007/978-3-319-24574-4_28
- Smit, P.B., & Janssen, T.T. (2019). Swell Propagation through Submesoscale Turbulence. *Journal of Physical Oceanography*, 49, 2615–2630. <https://doi.org/10.1175/JPO-D-18-0250.1>
- Smith, G. A., Hemer, M., Greenslade, D., Trenham, C., Zieger, S., & Durrant, T. (2021). Global wave hindcast with Australian and Pacific Island Focus: From past to present. *Geoscience Data Journal*, 8, 24–33. <https://doi.org/10.1002/gdj3.104>
- Song, Y., & Jiang, H. (2023). A Deep Learning–Based Approach for Empirical Modeling of Single-Point Wave Spectra in Open Oceans. *Journal of Physical Oceanography*, 53, 2089–2103. <https://doi.org/10.1175/JPO-D-22-0198.1>
- Woo, S., Park, J., Lee, J. Y., & Kweon, I.S. (2018). CBAM: Convolutional block attention module. In *Proceedings of the European Conference on Computer Vision (ECCV)* (pp. 3–19).
- The WAVEWATCH III® Development Group (WW3DG). (2019). User manual and system documentation of WAVEWATCH III® version 6.07. Tech. Note 333, NOAA/NWS/NCEP/MMAB, College Park, MD, USA, 326 pp. + Appendices.